Stabilization of Clusters by Interstitial Atoms. Three Carbon-Centered Zirconium Iodide Clusters, $Zr_6I_{12}C$, $Zr_6I_{14}C$, and $MZr_6I_{14}C$ (M = K, Rb, or Cs)

Jerome D. Smith and John D. Corbett*

Contribution from Ames Laboratory-DOE[1] and the Department of Chemistry, Iowa State University, Ames, Iowa 50011. *Received March 22, 1985*

Abstract: Well-faceted crystals of the title compounds are obtained in high yields by appropriate reactions of Zr, ZrI_4, graphite, and MI in sealed Ta tubes at 850 °C. Single-crystal X-ray diffraction studies, including an important correction for secondary extinction, established the presence of carbon in the center of all the Zr_6I_{12}-type clusters [Zr_6I_{14} and $MZr_6I_{14}C$ (M = Cs or $K_{0.58}$): space group *Cmca*, cluster symmetry $C_{2h} \simeq D_{2h}$; $Zr_6I_{12}C$, $R\bar{3}$, D_{3h}]. The $Zr_6I_{12}C$ and $CsZr_6I_{14}C$ compounds were previously misidentified as interstitial-free phases. The increase in cluster-based electrons from 14 to 16 in the above sequence is accompanied by a decrease in average Zr–Zr distances from 3.31 to 3.28 to 3.20 Å. Extended Hückel molecular orbital calculations have been used to study the bonding of terminal iodine atoms and the carbon atom as well as the source of cluster distortions. Although neglected in previous theoretical treatments, halogen atoms terminal to each metal atom in virtually all M_6X_{12} cluster compounds have a substantial effect on the radial component of the metal–metal bonding within the clusters. The orbital energies of the primary metal–metal bonding orbitals (and metal AO parentage) in $(Zr_6I_{12})(I^a)_6^{n-}$, n = 6–4, are ordered $a_{1g}(z^2) > t_{2g}(xz,yz) \simeq t_{1u}(xz,yz) > a_{2u}(xy)$. The addition of carbon to the cluster alters this through the formation of strongly bonding a_{1g} (with C 2s) and t_{1u} (C 2p) molecular orbitals. The inverse effect of distance to the terminal iodine atoms and thus Zr–I bond strength on metal–metal bonding within the cluster is responsible for the tighter cluster found in $Zr_6I_{12}C$ and for cluster distortions in other structures with asymmetric intercluster bridging.

Synthetic studies during the past decade to determine the composition, structures, and properties of reduced zirconium iodides have been prompted by the clear interrelationship that has been established between fission product iodine and the stress-corrosion cracking of zirconium-based fuel cladding in nuclear reactors.[2] The possible involvement of the abundant fission product cesium has also led us to the study of reduced phases in the ternary CsI–ZrI_4–Zr system. Among the several products found are a nonstoichiometric ZrI_3 in which chains of confacial ZrI_6 octahedra generate weakly interacting zirconium strings,[3,4] layered α- and β-ZrI_2,[5,6] dimeric $Cs_3Zr_2I_9$,[7] and two phases that contain Zr_6I_{12} clusters, reportedly Zr_6I_{12} and Cs-$(Zr_6I_{12})I_2$.[8,9]

Such cluster types are not entirely new inasmuch as several reduced halides of niobium and tantalum that contain M_6X_{12} clusters have been known for some time. Solid compounds of these clusters involve either ternary phases with isolated $(M_6X_{12})X_6^{n-}$ anions, n = 2–4, that is, with six terminal halide ligands,[10] or binary phases in which the clusters are linked through the shared terminal halide atoms, two structurally known examples having the stoichiometries M_6X_{14} and M_6X_{15}.[11-13] In all these compounds, between 14 and 16 electrons occupy 8 bonding orbitals derived mainly from metal d orbitals, a bonding scheme that has found support in theoretical considerations.[14,15]

In the past few years, M_6X_{12}-type clusters apparently containing only 9–12 electrons have also been reported for halides of transition metals to the left of group 5, namely, for zirconium, scandium, and several lanthanides.[8,9,16,17] These highly crystalline phases have typically been obtained in low yield from what were thought to be binary metal–halide reactions. However, reports have appeared more recently on the inclusion of second-period nonmetals both within octahedral metal clusters and chains of condensed octahedral clusters in rare earth metal halides[18-21] and in the two-dimensional sheets of condensed octahedral clusters in group 3 and 4 monohalides.[22-24] Accordingly, we are not only exploring new systems involving interstitial atoms but also reexamining some of the electron-poorer clusters mentioned above, especially those compounds for which residual electron density ($Z \sim$ 3–4) in the center of the cluster had been evident in single-crystal X-ray diffraction studies.

The $CsZr_6I_{14}$ phase was reexamined not only because a residual electron density had been found in the center of the cluster but also because the average Zr–Zr bond distances therein were 0.11 Å longer than those in Zr_6I_{12} even though the latter is only one electron more reduced. In addition, various preparations of $CsZr_6I_{14}$ have shown substantial variations in lattice dimensions as deduced by high-precision Guinier methods. The result of this study has been the synthesis and characterization of a series of zirconium iodide clusters containing carbon bound within the clusters: $Zr_6I_{12}C$, $Zr_6I_{14}C$, and $M^1Zr_6I_{14}C$ (M = K, Rb, or Cs). Interest in both the nature of the carbon bonding and structural

(1) Operated for the U. S. Department of Energy by Iowa State University under contract No. W-7405-Eng-82. This research was supported by the Office of Basic Energy Sciences, Materials Sciences Division.

(2) Cox, B.; Wood, J. C. "Corrosion Problems in Energy Conversion and Generation"; Tedmon, Jr., C. S.; Ed.; Electrochemical Society: New York, 1974, p 275.
(3) Daake, R. L.; Corbett, J. D. *Inorg. Chem.* **1978**, *17*, 1192.
(4) Larsen, E. M.; Wrazel, J. S.; Hoard, L. G. *Inorg. Chem.* **1982**, *21*, 2619.
(5) Guthrie, D. H.; Corbett, J. D. *J. Solid State Chem.* **1981**, *37*, 256.
(6) Corbett, J. D.; Guthrie, D. H. *Inorg. Chem.* **1982**, *21*, 1747.
(7) Guthrie, D. H.; Meyer, G.; Corbett, J. D. *Inorg. Chem.* **1981**, *20*, 1192.
(8) Corbett, J. D.; Daake, R. L.; Poeppelmeier, K. R.; Guthrie, D. H. *J. Am. Chem. Soc.* **1978**, *100*, 652.
(9) Guthrie, D. H.; Corbett, J. D. *Inorg. Chem.* **1982**, *21*, 3290.
(10) Koknat, F. W.; McCarley, R. E. *Inorg. Chem.* **1974**, *13*, 295.
(11) Simon, A.; von Schnering, H.-G.; Wöhrle, H.; Schäfer, H. *Z. Anorg. Allg. Chem.* **1965**, *339*, 155.
(12) Bauer, D.; von Schnering, H.-G.; Schäfer, H. *J. Less-Common Met.* **1965**, *8*, 388.
(13) Bauer, D.; von Schnering, H.-G. *Z. Anorg. Allg. Chem.* **1968**, *361*, 259.
(14) Cotton, F. A.; Haas, T. E. *Inorg. Chem.* **1964**, *3*, 10.
(15) Robbins, D. J.; Thomson, A. J. *J. Chem. Soc., Dalton Trans.* **1972**, 2350.
(16) Corbett, J. D.; Poeppelmeier, K. R.; Daake, R. L. *Z. Anorg. Allg. Chem.* **1982**, *491*, 51.
(17) Berroth, K., Dissertation, University of Stuttgart, 1980.
(18) Warkentin, E.; Masse, R.; Simon, A. *Z. Anorg. Allg. Chem.* **1982**, *491*, 323.
(19) Warkentin, E., Simon, A. *Rev. Chim. Miner.* **1983**, *20*, 488.
(20) Hwu, S.-J.; Corbett, J. D.; Poeppelmeier, K. R. *J. Solid State Chem.* **1985**, *57*, 43.
(21) Ziebarth, R. P.; Corbett, J. D. *J. Am. Chem. Soc.* **1985**, *107*, 4571.
(22) Seaverson, L. M.; Corbett, J. D. *Inorg. Chem.* **1983**, *22*, 3202.
(23) Ford, J. E.; Corbett, J. D.; Huw, S.-J. *Inorg. Chem.* **1983**, *22*, 2789.
(24) Ziebarth, R. P.; Hwu, S.-J.; Wijeyesekera, S. D.; Corbett, J. D., unpublished research.

0002-7863/85/1507-5704$01.50/0

Table I. Stronger Lines in the Guinier Powder Patterns for $CsZr_6I_{14}C$, $Zr_6I_{14}C$, and $Zr_6I_{12}C$[a]

$CsZr_6I_{14}C$						$Zr_6I_{14}C$	$Zr_6I_{12}C$					
h	k	l	$2\theta_{obsd}$	$2\theta_{calcd}$	I_{calcd}	I_{calcd}	h	k	l	$2\theta_{obsd}$	$2\theta_{calcd}$	I_{calcd}
1	1	1	10.72	10.78	19	85	1	0	1		11.29	15
3	1	2		22.62	11	13	1	1	0	12.15	12.19	6
4	2	1	26.67	26.66	35	47	0	0	3	26.69	26.70	15
0	0	4	27.56	27.56	35	36	1	3	1	27.06	27.07	45
0	4	2	*b*	28.50	81	86	1	3	−2	31.25	31.25	100
4	2	2	29.26	29.26	100	95	1	3	4	44.54	44.55	32
0	4	3	32.52	32.59	30	34	5	2	0	45.01	45.02	32
4	2	3	33.19	33.18	82	100	1	3	−5	52.67	52.70	11
1	5	2	34.74	34.72	11	13	5	2	3	53.09	53.11	10
1	1	5	35.72	35.70	13	9	2	6	−1	53.32	53.32	10
4	2	4	38.06	38.07	17	14	2	6	2	55.80	55.82	15
4	2	5	43.68	43.66	22	22	2	6	−4	65.16	65.19	11
4	6	0	44.35	44.34	51	45	1	3	7	71.19	71.24	7
8	0	0	45.89	45.90	27	25	2	6	5	71.73	71.77	6
0	4	6	49.33	49.32	22	23	5	2	6	73.67	73.62	6
4	2	6	49.81	49.80	29	24	9	1	2	74.42	74.39	6
4	6	4	52.99	53.02	27	23						
8	0	4	54.39	54.38	13	11						
8	4	2	54.92	54.92	27	25						
0	0	8	56.90	56.90	12	9						
8	4	3	57.34	57.36	10	8						

[a] $CuK\alpha_1$ radiation, Guinier polarization. [b] Interference from Si standard.

differences between the two types of carbide clusters in these also prompted an extended Hückel MO study of these systems, including effects of bonding of the inevitable terminal halide atoms found about M_6X_{12} clusters.

Experimental Section

Materials. The purity, preparation, and handling of reactor-grade Zr and ZrI_4 have been previously described.[5] Zirconium powder was prepared from metal strips via ZrH_{2-x} as previously described.[20] Reagent-grade alkali-metal iodides were distilled under vacuum prior to use. Spectroscopic-grade graphite powder (National Brand, Union Carbide) and 99% ^{13}C graphite (MSD ISOTOPES) were degassed under vacuum at 850 °C prior to use.

Synthesis. All reactions were run in sealed Ta tubes by using techniques described previously.[6,22] Reactions involving a number of potential interstitial impurities were explored, especially for the ubiquitous oxygen, but carbon proved to be by far the most productive. The indicated yields were generally estimated both from careful powder pattern analysis and visually, the black products of interest often appearing as well-faceted and gem-like crystals up to 0.4 mm in diameter that grew in both clumps and as separate crystals on both the Zr metal and the Ta container. Well-crystallized samples of $CsZr_6I_{14}C$ and $RbZr_6I_{14}C$ were produced in >90% yield by reaction of stoichiometric quantities of Zr powder, ZrI_4 (~400 mg), graphite, and CsI or RbI at 850 °C for 2 weeks. $CsZr_6I_{14}C$ has also been made in essentially quantitative yield in reactions containing an excess of Zr strips under the same conditions. A structural analysis of the cesium product showed that the compound was stoichiometric in alkali metal, and the same was inferred for the rubidium compound based on lattice constants. However, reactions run with substoichiometric amounts of CsI resulted in large yields of products with smaller lattice parameters, implying that less than full cesium occupancy is also possible. Reactions loaded to form fully stoichiometric $KZr_6I_{14}C$ resulted in a 90% yield of a material that turned out to be potassium deficient, $K_{0.58}Zr_6I_{14}C$, according to a single-crystal diffraction study. Similar yields of $KZr_6I_{14}C$, which was presumably fully stoichiometric judging from the appropriately larger lattice constants, were obtained when a 2-fold excess of KI was included in the reaction. The corresponding phase could not be obtained with NaI, LiI, or BaI_2.

The phase $Zr_6I_{14}C$ was synthesized in 70–80% yield from stoichiometric quantities of ZrI_4 (~400 mg), Zr, and C that were allowed to react at 850 °C for 1 week and the products ground and then reequilibrated at 850 °C for an additional week; the remaining iodide product was ZrI_3. The phase has also been observed as the only iodine-containing product from reactions of equimolar amounts of zirconium, iodine, and carbon, ZrC also being produced. $Zr_6I_{12}C$ was similarly formed in high yield when excess Zr in the form of either strips or powder was employed in reactions of 2-weeks duration at 850 °C. It is also obtained by allowing the layered α- or β-ZrI_2 to react with the stoichiometric amount of graphite under the same conditions.

The good yields, the high crystallinity of the products of interest, and their distribution about the reaction tube suggest vapor-phase transport processes. The $Zr_6I_{14}C$ and $CsZr_6I_{14}C$ crystals were generally unreactive toward air and water at room temperature. The same was true of $Zr_6I_{12}C$, as noted before,[9] but only in some cases; other samples reacted fairly rapidly with water to give a greenish-black suspension and a detectible odor of acetylene. We believe that this difference is associated with different degrees of perfection of the crystals, dependent at least in part on the rate of their growth.

X-ray Powder Diffraction. Preliminary product identification utilized X-ray powder data obtained with a focusing Guinier camera (Enraf-Nonius) equipped with a silicon monochromator to give clean Cu $K\alpha_1$ radiation. Sample mounting has been previously described.[3] NBS silicon (SRM-640) was included as an internal standard, the five observed silicon lines being fitted by least squares to known diffraction angles with a quadratic function in position. The powder patterns were indexed with the aid of data calculated for known structures, and lattice constants were determined by standard least-squares refinement. The stronger diffraction lines calculated for $CsZr_6I_{14}C$ and the closely related $Zr_6I_{14}C$ and $Zr_6I_{12}C$ are listed in Table I.

The lattice parameters of all phases were very reproducible if enough alkali-metal iodide was added when appropriate to ensure full occupancy of the cation site. No evidence for the nonstoichiometry of carbon was found. The yields of carbide products from reactions that were deficient in carbon were roughly proportional to the amount of carbon added while the lattice parameters of the resulting phases were not significantly different from those of the same materials produced in high yield.

Magnetic Susceptibility. The magnetic susceptibility of $CsZr_6I_{14}C$ was measured from 95 to 298 K by using the Faraday method. The sample was contained in a screw-top Teflon bucket suspended from the balance by a tungsten wire. The bucket and wire were calibrated at the above temperatures to correct for their magnetic effects. A more complete description of the balance can be found elsewhere.[25] The susceptibility data were initially fit to a Curie model. The temperature-independent term was then subtracted from each datum, and the data were refit to the Curie–Weiss law.

Single-Crystal X-ray Studies. Reaction containers were opened in a drybox equipped with a nearly horizontal window above which an ordinary binocular microscope was mounted, and crystals were mounted in a thin-walled glass capillaries, typically 0.3-mm i.d. All single-crystal X-ray diffraction data sets were collected on a Syntex $P2_1$ diffractometer using Mo $K\alpha$ radiation (no monochromator, Zr filter to eliminate Mo $K\beta$) and $2\theta/\omega$ scans. A summary of the details of the single-crystal investigations is given in Table II. An empirical absorption correction was carried out with the aid of full-circle ϕ-scan data obtained on the diffractometer. As referenced before,[20] the absorption correction program was ABSN, and structure factor calculations and full-matrix least-squares refinements were done by using the program ALLS, Fourier synthesis with FOUR, and drawings with the program ORTEP. Atomic scattering factors included corrections for the real and imaginary contributions to anomalous dispersion.[26]

(25) Stierman, R. J.; Gschneidner, K. A., Jr.; Tsang, T.-W. E.; Schmidt, F. A.; Klavins, P., Shelton, R. N.; Queen, J.; Legvold, S. *J. Magn. Mat.* **1983**, *36*, 249.

Table II. Crystallographic Data for Single-Crystal Investigations

	$Zr_6I_{14}C$	$K_{0.58}Zr_6I_{14}C$	$CsZr_6I_{14}C$	$Zr_6I_{12}C$
space group	*Cmca*	*Cmca*	*Cmca*	$R\bar{3}$
Z	4	4	4	3
cryst dimens, mm	0.20 × 0.20 × 0.16	0.24 × 0.18 × 0.14	0.30 × 10.16 × 0.20	
$2\theta_{max}$, deg	55	55	55	65
reflectns				
measd	3776	3761	3644	4160
obsd[a]	1785	1927	1969	2558
indepen	931	1025	1068	883
R_{av} (%)	2.9	2.6	2.3	3.2
R^b (%)	3.6	3.6	3.3	3.2
$R_w{}^c$ (%)	4.5	4.2	3.9	4.2
secondary extinct. coeff (10^{-4})	1.2 (2)	4.5 (4)	2.7 (3)	2.0 (1)
absorpt coeff μ, 1/cm	173	173	182	178
range of transm. coeff	0.81–1.00	0.55–1.00	0.81–1.00	0.77–1.00
no. of param	90	101	101	46
no. of variab	52	54	56	30

[a] $F_{obsd} \geq 3\sigma_F$ and $I_{obsd} > 3\sigma_I$. [b] $R = \sum(|F_o| - |F_c|)/\sum|F_o|$. [c] $R_w = [\sum w(|F_o| - |F_c|)^2/\sum w|F_o|^2]^{1/2}$.

The general observation that $F_{calcd} > F_{obsd}$ for large F and the fact that the crystals used were well-formed and faceted indicated the data warranted the inclusion of a secondary extinction correction,[27] and this turned out to be vital in the correct refinement of the interstitial carbon (or other) atom at the center of symmetry within the clusters. A careful analysis of the Fourier synthesis output for the two space groups involved revealed that the large structure factors contribute significant electron density at the cluster center (D_{3h} and C_{2h} point symmetries). Therefore, small negative errors in these F's have a marked effect of like sign on the magnitude of an atom refined at this position, even to the point that no interstitial atom is indicated by a Fourier synthesis using data from a well-formed crystal without this correction.

In each refinement, the Zr and I positions from a previously determined structure[9] were used as a model from which to begin refinement. An electron density map was then used to determine whether an atom was present in either the center of the cluster or in interstices within the iodine array known (or likely) to be occupied by alkali-metal atoms or both. These atoms were then included as appropriate, and subsequently all unique positional and anisotropic thermal parameters (isotropic for C) together with the occupancy of the alkali metal, if any, were refined. Only with the potassium salt was the last significantly different from unity. In all cases, the isotropic B for carbon initially refined to a value near or below zero (but not significantly so) when the occupancy of the carbon was held at unity, suggesting that slightly more electron density was present than accounted for by a single carbon. However, the data showed a significant dependence of $\sum w(|F_o| - |F_c|)^2$ on F_o, a reweighting of the data in 10–15 overlapping groups sorted on F_o with a statistically meaningful procedure[28] corrected both problems, and the carbon's isotropic B thereafter remained positive in all cases. Final electron density difference maps were flat everywhere to within the equivalent of $Z = \pm 0.5$.

Extended Hückel Calculations. To understand the bonding in these interstitial clusters more fully, noninterative extended Hückel calculations[29,30] were carried out on isolated $Zr_6I_{12}^{2+}$, $Zr_6I_{18}^{4-}$, and $Zr_6I_{18}C^{4-}$ clusters with dimensions for the latter two as observed in $Zr_6I_{14}C$ except that very small changes were made to give the clusters D_{2h} symmetry rather than the lower crystallographic C_{2h} point symmetry. The Cartesian coordinates of the atoms in these clusters and the variables describing the radial extension and energies of the atomic orbitals (Zr, s,p,d; I, s,p) are available in the supplementary material.

Results and Discussion

The investigation was initially targeted on the cause(s) for the variability in the lattice parameters of and the residual electron density within the clusters in the reported $CsZr_6I_{14}$ structure. This established the presence, even the necessity, of small interstitial atoms within the clusters and led to the synthesis and characterization of a series of compounds containing carbon-centered $Zr_6I_{12}C$ clusters: $Zr_6I_{14}C$, $K_{0.58}Zr_6I_{14}C$, $MZr_6I_{14}C$ (M = Cs, Rb, or K), and $Zr_6I_{12}C$. There are good indications that this is only the beginning of a substantial interstitial chemistry for zirconium clusters.[21,31,32] All the above cluster carbides were obtained in high yields and as well-formed crystals from reactions of ZrI_4.

Table III. Cell Parameters (Å) and Volumes (Å^3) of Zirconium Iodide Cluster Compounds[a]

compd	a	b	c	V
$Zr_6I_{14}C$	15.690 (3)	14.218 (3)	12.808 (3)	2857 (1)
$K_{0.58}Zr_6I_{14}C$	15.727 (2)	14.278 (3)	12.798 (2)	2874 (1)
$KZr_6I_{14}C$	15.757 (2)	14.314 (2)	12.807 (2)	2889 (1)
$RbZr_6I_{14}C$	15.768 (2)	14.296 (2)	12.849 (2)	2896 (1)
$CsZr_6I_{14}C$	15.803 (2)	14.305 (3)	12.934 (1)	2924 (1)
$Zr_6I_{12}C$	14.508 (1)		10.007 (1)	1824 (1)
"$CsZr_6I_{14}$"[b]	15.83–15.94	14.29–14.33	12.94–12.99	2930-2958
"Zr_6I_{12}"[c]	14.502 (2)		9.996 (2)	1821 (1)

[a] The $MZr_6I_{14}X$ phases are orthorhombic, space group *Cmca*, and $Zr_6I_{12}X$ $R\bar{3}$, which is reported here in the hexagonal setting. All data from Guinier powder diffraction unless otherwise noted. [b] The range of values found in previous investigations, with values near the lower limit pertaining to the reported structure.[9] [c] Lattice parameters obtained with Ames Laboratory diffractometer, which characteristically yields smaller results by close to the amount shown.

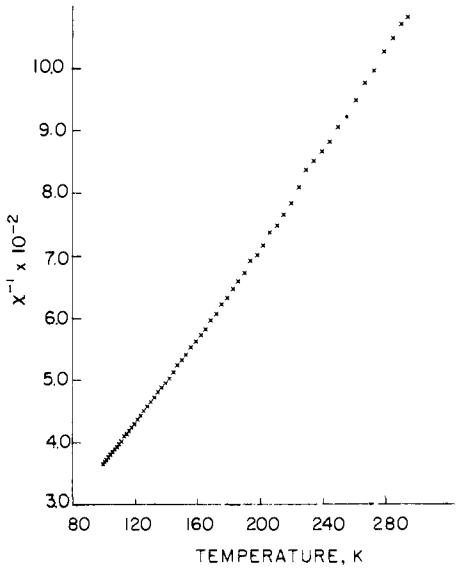

Figure 1. Reciprocal molar magnetic susceptibility vs. temperature (K) for $CsZr_6I_{14}C$, corrected for core diamagnetism and temperature-independent paramagnetism ($\mu \sim 1.48\ \mu_B$, $\theta = -6$ K).

(26) "International Tables for X-ray Crystallography"; Kynoch Press: Birmingham, England, 1968 and 1974; Vols. III and IV.
(27) Coppens, P., Hamilton, W. C. *Acta Crystallogr., Sect. A* **1970**, *A26*, 71.
(28) Hubbard, C. R.; Jacobson, R. A., Ames Laboratory, unpublished program, 1969.
(29) Hoffmann, R. *J. Chem. Phys.* **1963**, *39*, 1397.
(30) Hoffmann, R.; Lipscomb, W. N. *J. Chem. Phys.* **1962**, *36*, 2179, 2189.
(31) Smith, J. D.; Corbett, J. D. *J. Am. Chem. Soc.* **1984**, *106*, 4618.
(32) Smith, J. D.; Corbett, J. D. *J. Am. Chem. Soc.*, to be submitted.

Table IV. Atomic Positions for Zr–I–C Clusters

	x	*y*	*z*
		$Zr_6I_{14}C$	
I1	0.12943 (6)	0.09099 (6)	0.24965 (9)
I2	0.12541 (5)	0.25704 (7)	0.00898 (8)
I3	$^1/_4$	0.34773 (9)	$^1/_4$
I4	0	0.1530 (1)	0.7665 (1)
I5	0.24622 (9)	0	0
Zr1	0.39308 (8)	0.0639 (1)	0.8901 (1)
Zr2	0	0.3657 (1)	0.9028 (2)
C	$^1/_2$	$^1/_2$	$^1/_2$
		$K_{0.58}Zr_6I_{14}C$	
I1	0.12498 (4)	0.09064 (5)	0.24860 (7)
I2	0.12568 (4)	0.25754 (5)	0.0089 (6)
I3	$^1/_4$	0.34852 (8)	$^1/_4$
I4	0	0.15407 (7)	0.76624 (9)
I5	0.24644 (6)	0	0
K[a]	0	0	0
Zr1	0.39406 (6)	0.06342 (8)	0.8901 07 (9)
Zr2	0	0.3671 (1)	0.9030 (1)
C	$^1/_2$	$^1/_2$	$^1/_2$
		$CsZr_6I_{14}C$	
I1	0.12536 (4)	0.08999 (4)	0.25040 (5)
I2	0.12574 (4)	0.25739 (4)	0.00594 (5)
I3	$^1/_4$	0.34908 (6)	$^1/_4$
I4	0	0.15832 (6)	0.76052 (7)
I5	0.24756 (6)	0	0
Cs	0	0	0
Zr1	0.39486 (6)	0.06363 (7)	0.89269 (7)
Zr2	0	0.36805 (9)	0.9031 (1)
C	$^1/_2$	$^1/_2$	$^1/_2$
		$Zr_6I_{12}C$	
I1	0.035525 (4)	0.10257 (4)	0.33250 (6)
I2	0.12642 (4)	0.17766 (4)	0.32488 (6)
Zr	0.14301 (6)	0.04066 (6)	0.13012 (8)
C	0	0	0

[a] Occupancy = 0.58 (3).

Zr, graphite, and alkali-metal iodides where needed at 850 °C for 1–2 weeks. The use of insufficient carbon always resulted in an appropriately reduced yield of the cluster phase. Lattice parameters for the carbon-containing phases synthesized here as well as for the previously reported zirconium iodide cluster phases are given in Table III. No variability in these was found for any of the carbides except for a significant decrease in cell volume for $MZrI_{14}C$ phases when insufficient alkali-metal iodide was included in the reaction, as shown for $K_{0.58}Zr_6I_{14}C$.

The expected paramagnetic nature of $CsZr_6I_{14}C$ has been confirmed by magnetic susceptibility measurements. As seen in Figure 1, the material exhibits Curie–Weiss behavior between 100 and 298 K to yield $\theta = -6$ K and a $\mu = 1.48\ \mu_B$ that is appropriate for one unpaired and delocalized electron per cluster[33] (a_{2u}^1—below). The phase shows no EPR signal at room temperature, 77 K, or even at 4 K between 0 and 13 kG. Presumably this arises from very rapid electron spin–lattice relaxation, but a magnetic transition below 100 K has not been ruled out. (The cluster compound Nb_6I_{11}, magnetically a quartet at room temperature,[34] is also without an EPR signal.)

The structures of four of these phases—$Zr_6I_{14}C$, $K_{0.58}Zr_6I_{14}C$, $CsZr_6I_{14}C$, and $Zr_6I_{12}C$—were determined by single-crystal X-ray diffraction. The final refined atomic coordinates and their standard deviations are compiled in Table IV for each structure. The final anisotropic thermal parameters and the observed and calculated structure factor amplitudes are available as supplementary material. Table V contains the important bond lengths in the structures. The isolated clusters in the two structure types, $Zr_6I_{12}C$ and $(M)Zr_6I_{14}C$, are shown in Figure 2.

The information gained from the present synthetic and single-crystal structural studies elucidates the relationship between the carbon-containing clusters reported here and the nominal binary clusters obtained earlier.[9] The phase "Zr_6I_{12}" prepared before from ZrI_4 and excess metal but only in low and erratic yields was evidently $Zr_6I_{12}C$ which can be obtained in high yield with carbon as a reactant. All bond distances and angles found for the two materials agree to within $2–3\sigma$, while the slight differences observed in lattice parameters are typical and arise because of differences in data sources (Table III). Repeated attempts to obtain a rhombohedral phase with other dimensions have been unsuccessful although it was possible to obtain the previously unidentified $Zr_6I_{14}C$. We suspect that an interstitial atom, probably carbon, was not evident in the previous "Zr_6I_{12}" because of both the relatively poor quality of the diffraction data ($R = 0.11$) and a possible systematic negative error in electron density at that position that would arise from an insufficient correction for secondary extinction (see Experimental Section). Indeed, a peak in the center of the present cluster did not appear in a Fourier synthesis using the otherwise refined parameters until the extinction correction was applied.

To appreciate how little carbon is required for the stoichiometric reaction, it is only necessary to observe that the compound $Zr_6I_{12}C$ contains just 0.58% carbon by weight. The highly crystalline nature of the phase and its habit of growing as well-formed crystals on the surface of the metal strips allow the ready isolation of single crystals when the total yield is below 5%. The source of the small amount of carbon required to observe this amount in a "binary" reaction is naturally difficult to determine. Foremost among the suspected problems is the difficulty of rinsing all traces of tantalum cleaning solution from the crimped and welded end of the reaction tube before this is loaded and sealed. The observation of a possible impurity-stabilized phase in small yield, followed by its synthesis in large yield when the correct impurity is purposefully added, has already been noted with $Sc_7Cl_{10}C_2$[20] and with layered

Table V. Bond Distances in Zirconium Iodide Cluster Phases (Å)

	$Zr_6I_{14}C$	$K_{0.58}Zr_6I_{14}C$	$CsZr_6I_{14}C$	$Zr_6I_{12}C$
		Zr–Zr Intralayer[a]		
Zr1–Zr1	(×2) 3.355 (3)	3.332 (2)	3.324 (2)	(×6) 3.200 (1)
Zr1–Zr2	(×4) 3.284 (2)	3.264 (2)	3.257 (2)	
		Zr–Zr Interlayer		
Zr1–Zr1	(×2) 3.345 (3)	3.325 (2)	3.321 (2)	(×6) 3.190 (1)
Zr1–Zr2	(×4) 3.292 (2)	3.272 (2)	3.270 (2)	
Zr1–Zr1	(×2) 4.738 (3)	4.707 (2)	4.699 (2)	(×3) 4.518 (1)
Zr2–Zr2	(×1) 4.560 (4)	4.536 (3)	4.530 (2)	
		$Zr–I^i$		
Zr1–I5	(×2) 2.847 (2)	2.855 (1)	2.860 (1)	
Zr1–I1	(×2) 2.860 (2)	2.872 (1)	2.884 (1)	(×6) 2.861 (1)[b]
Zr1–I2	(×2) 2.868 (2)	2.881 (1)	2.895 (1)	(×6) 2.873 (1)
Zr2–I1	(×2) 2.840 (2)	2.852 (1)	2.862 (1)	
Zr2–I2	(×2) 2.848 (2)	2.856 (1)	2.867 (1)	
		$Zr–I^{i-a}$		
Zr1–I4	(×2) 2.908 (2)	2.916 (1)	2.920 (1)	(×6) 2.940 (1)[b]
				(×6) 2.912 (1)
		$Zr–I^{a-i}$		
Zr2–I4	(×2) 3.491 (3)	3.509 (2)	3.522 (2)	(×6) 3.403 (1)[b]
		$Zr–I^{a-a}$		
Zr1–I3	(×4) 3.138 (2)	3.158 (1)	3.195 (1)	
		Zr–C		
Zr1–C	(×4) 2.369 (2)	2.354 (1)	2.349 (1)	(×6) 2.259 (1)
Zr2–C	(×2) 2.280 (1)	2.268 (1)	2.265 (1)	
		M–I		
M–I1	(×4)	3.957 (1)	4.010 (1)	
M–2I	(×4)	4.176 (1)	4.185 (1)	
M–I4	(×2)	3.713 (1)	3.837 (1)	
M–I5	(×2)	3.876 (1)	3.914 (1)	

[a] Referred to approximately close-packed layers that run roughly horizontally and perpendicular to the page in Figure 2.[9] [b] In Zr_6I_{12}, the $Zr–I^i$ distances are all Zr1–I2 while the $Zr–I^{i-a}$ and $Zr–I^{a-i}$ distances are both Zr1–I1.

(33) Converse, J. G.; McCarley, R. E. *Inorg. Chem.* **1970**, *9*, 1361.
(34) Finley, J. J.; Comley, R. E.; Vogel, E. E.; Zevins, V.; Gmelin, E. *Phys. Rev. B* **1981**, *24*, 1023.

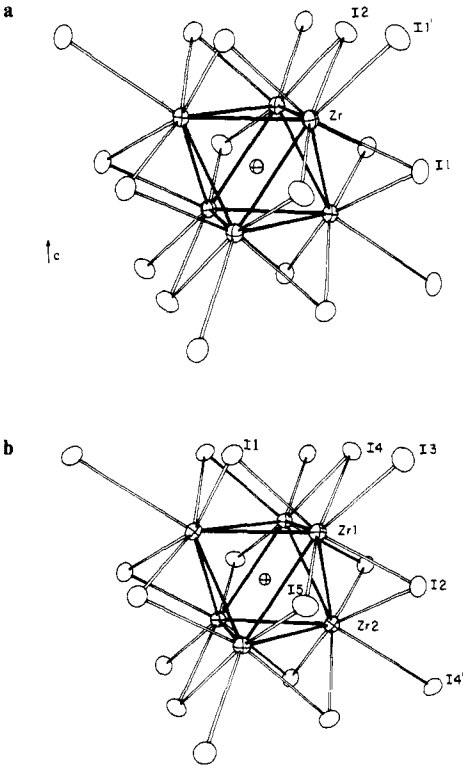

Figure 2. Isolated clusters in (a, top) $Zr_6I_{12}C$ (D_{3h} point symmetry) and (b, bottom) $CsZr_6I_{14}C$ (C_{2h}) with the c axes approximately vertical. In $Zr_6I_{12}C$, the exo I1′ = I^{a-i} iodine atoms are I1 in other clusters; in $CsZr_6I_{14}C$, a 2-fold axis passes through I5 and C and a mirror plane through I4, C, and Zr2, with I3 = I^{a-a}, I4 = I^{i-a}, I4′ = I^{a-i} from other clusters, and the remainder I^i. The carbon lies at an inversion center (75% thermal ellipsoids).

M^I_xYClO, M'_2Cl_2C (M′ = Y, Sc, or Zr), and M″ClH (M″ = Y or Sc) phases.[23,24]

The relationship between $CsZr_6I_{14}C$ and the published "$CsZr_6I_{14}$" is not so obvious, but it appears likely that some amount of a different interstitial atom together with a cesium substoichiometry may have been involved. The Zr–Zr distances in the earlier "$CsZr_6I_{14}$" are 0.02–0.03 Å greater and the cell volume is significantly larger than that found for $CsZr_6I_{14}C$, although the Zr–I^i separations differ by ≤0.01 Å. Other interstitials that may be involved have been investigated, and reports on these will be forthcoming.[32]

It is obvious that the presence of interstitial carbon in these clusters markedly enhances yields of the so-called lower zirconium iodides and improves their apparent thermodynamic stability. The synthesis of the alternative α- and β-ZrI_2 with the same or lower oxidation state and only zigzag metal chains usually is achieved in moderately low yield unless much excess metal is present. At the present time, we conclude that empty zirconium iodide cluster compounds do not exist, and this probably also pertains to the chlorides.[24]

Structural Results. Both $Zr_6I_{12}C$ and $MZr_6I_{14}C$ (M = K, Rb, Cs, and nothing) are based on $Zr_6I_{12}C$ clusters composed of a slightly distorted metal octahedron centered by a carbon atom and with 12 inner (i) iodine atoms bridging each of the edges of that octahedron. As with virtually all clusters and their condensation products, each zirconium is also bonded to an outer (a = äussere) iodine that always occupies a terminal or exo position on each vertex of the octahedron so that the carbon, the zirconium and this terminal iodine are nearly colinear. Each cluster would then be described as $Zr_6I^i_{12}I^a_6C$. However, the actual stoichiometries of the basic M_6X_{12} and M_6X_{14} structure types are the result of the three-dimensional way in which the clusters are interconnected through shared iodines to eliminate some or all the I^a atoms. Full descriptions of this interconnectivity have appeared previously,[9,11,12] but a brief description will be included here because this secondary bonding is important in understanding the closely interrelated bonding of the interstitial carbon atom as well as the source of cluser distortions.

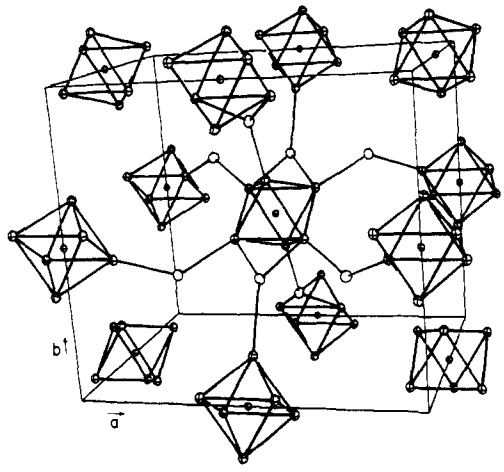

Figure 3. Interconnectivity of the Zr_6I_{12} clusters in $Zr_6I_{14}C$ with iodine atoms as open ellipsoids. All edge-bridging I^i not involved in intercluster bridging have been omitted for clarity.

In $Zr_6I_{12}C$, the octahedra are cubic-close-packed with the 3-fold axes in each and the iodine layers lying parallel and normal to the $\vec{c}$ direction of the hexagonal cell, respectively. The six I^i (I1) atoms that bridge the edges around the waist of the cluster, Figure 2a, are three-coordinate as they also serve as more distant terminal iodines in adjacent clusters. A useful formulation of this interconnectivity is $Zr_6I^i_6I^{i-a}{}_{6/2}I^{a-i}{}_{6/2}C$, where I^{i-a} refers to the functionality described in the previous sentence. The cluster is slightly compressed along the $\bar{3}$ axis, a distortion that probably reflects the extra bonding of the waist iodine atoms.

The interconnectivity accompanying the stoichiometry of the isostructural $Zr_6I_{14}C$ and $MZr_6I_{14}C$ phases is more complex, and the symmetry of the cluster is accordingly lower. In this case, 10 of the 12 edges of each nominal metal octahedron are bridged by inner iodines (I1,2,5, Figure 2*b*) that belong only to this cluster. The remainder of the iodine atoms are involved in intercluster bridging to all terminal positions on this or other metal octahedra, and only these are shown in Figure 3. The two remaining and opposed edges are bridged by inner iodines that are also terminal to zirconium in two adjacent clusters. Likewise, two of the metal atoms in this cluster are distantly bound (~3.5 Å) to inner iodines on adjacent clusters, all four of these bifunctional I4 atoms lying on a mirror plane. Four additional iodines (I3) serve only to bridge to similar terminal positions on adjacent clusters (d(Zr–I) = 3.14–3.20 Å). The formulation of the interconnectivity of these phases is thus $[Zr_6I^i_{10}I^{i-a}{}_{2/2}I^{a-i}{}_{2/2}I^{a-a}{}_{4/2}C]$. Finally, the interstice at the origin surrounded only by iodine atoms is occupied by Cs, Rb, K, or nothing depending on the composition. The metal octahedra in 6–14 phases show a marked compression (0.08–0.09 Å) along a pseudo-4-fold axis defined by two zirconium atoms (Zr2) that are bound to the terminal I^{a-i} atoms (I4) (Figure 3). This distortion will be seen to be a logical consequence of the weaker bonding to the more distant terminal iodine atoms. These 6–14 carbide phases are isostructural with the long-known[11,12] Nb_6Cl_{14} and Ta_6I_{14} when one excludes the alkali-metal and carbon atoms.

Carbon 13 in $CsZr_6I_{14}{}^{13}C$ exhibits a single tensor in the NMR spectrum that can be well described in terms of axially symmetry shielding with $\sigma_\parallel$ and $\sigma_\perp$ components of 15 and 54 ppm (vs. TMS). This is very consistent with the symmetry about carbon in the structure reported here and leaves little doubt that the interstitial atom has been correctly identified. On the other hand, only a very broad signal could be observed for $Zr_6I_{12}{}^{13}C$.[35]

The intercomparison of distances between these structures and other reduced zirconium halides is made difficult in part by matrix

(35) Fry, C. G.; Smith, J. D.; Gersteln, B. C.; Corbett, J. D. *Inorg. Chem.*, submitted.

effects,[36] which in this instance are the presumed limitations on the optimal zirconium–zirconium and zirconium–carbon bonding that originate from substantial closed-shell repulsions between the large and rather tightly packed iodines, particularly among those in the inner, edge-bridging core in $Zr_6I_{12}C$ but also in limiting the approach of I^a. An apparent matrix effect can be seen in both clusters in Figure 2 where the zirconium atoms clearly lie inside the planes defined by the four neighboring I^i atoms. The observed result amounts to a compromise between diminished Zr–I overlap and an increased Zr–Zr and Zr–C bonding that accompany the distortion from the idealized M_6X_{12} cluster.

The metal–metal part of the bonding of course also depends on electron count and the number of metal neighbors, and so direct metal–metal distance comparisons between diverse structures even in the absence of matrix problems is not particularly useful except in a total bond order sense.[36] The fact that Zr–Zr and $Zr–I^{a-a}$ distances (Table V) decreases and increase, respectively, with increasing electron count, with a sizable drop in the former on reaching $Zr_6I_{12}C$, will be considered shortly in connection with bonding descriptions. It is interesting that the average Zr–Zr distance in the last, 3.195 Å, is very close to the 3.201-Å value in $Zr_6Cl_{12}{\cdot}K_2ZrCl_6$.[37]

The zirconium–carbon distances in the present series average 2.34 Å in $Zr_6I_{14}C$, 2.32 Å in the cesium salt, and 2.26 Å in the generally more tightly bound $Zr_6I_{12}C$, a more-or-less reasonable reduction, the various values comparing well with the 2.342-Å separation in ZrC (NaCl type).[38] A 2.32-Å Zr–C distance is estimated from the six-coordinate crystal radius[39] for Zr^{IV} and an average value of 1.46 Å for the carbon radius deduced from a number of rock-salt-type monocarbides of the earlier transition metals with the aid of standard cation crystal radii, a procedure that generally seems to describe interstitial-metal distances fairly well, in $Sc_7Cl_{10}C_2$ for example.[20,24]

The observed cesium–iodine separation, 4.02 Å for 12 neighbors, is 0.06 Å less than the sum of the 12-coordinate radii but reasonable for iodine also bound to zirconium, while this separation in the substoichiometric potassium phase has only decreased to 3.98 Å, 0.14 Å *greater* than the sum of standard radii. This small decrease in cavity size is appropriate for a somewhat rigid $Zr_6I_{14}C$ matrix into which cations may be substituted. The poorer-binding thus-afforded potassium presumably is responsible for the larger thermal ellipsoid observed for it, 6.9 $Å^2$, and may account for both the substoichiometry achieved under normal circumstances and our inability to synthesize the sodium, lithium, or barium derivatives. The last would afford the filled 16-electron cluster (below) except that the standard radius for Ba^{2+} is about 0.03 Å smaller than for K^+, and this cation is probably less forgiving of poor coordination.

Cluster Bonding. The nature of the bonding in these interstitial-stabilized cluster can be examined in two ways. The first is the empirical observation of changes in structural parameters on reduction from $Zr_6I_{14}C$ to $M^1Zr_6I_{14}C$ to $Zr_6I_{12}C$ as well as the consideration of differences in the individual clusters in the distinct structural matrices provided in $Zr_6I_{12}C$ and $M_xZr_6I_{14}C$. The second approach to cluster bonding has been the application of extended Hückel methods, the results of which lead to an appreciation of both the manner in which carbon stabilizes the clusters and the significance of the structural and electronic changes reflected in differences in distances.

With the plausible assumption that the iodine valence bands are filled, there are 14 electrons in $Zr_6I_{14}C$, 15 in $M^1Zr_6I_{14}C$, and 16 in $Zr_6I_{12}C$ available from the carbon and zirconium for cluster bonding. The observed effect of this increase is a decrease in the average Zr–Zr bond distance from 3.309 (3) Å in $Zr_6I_{14}C$ to 3.283 (2) Å in $CsZr_6I_{14}C$ and 3.195 (1) Å in $Zr_6I_{12}C$. These changes are considerably greater than the overall result reflected in just the cell volumes (Table I). The much larger decrease in the last step of the reduction arises partially because of the bonding character of the orbital being filled but, more importantly, also because of basic differences in the two structures, as will be considered later. As seen in Table V, there is a much less dramatic increase in $Zr–I^i$ and $Zr–I^{a-a}$ distances through the same series, while the erratic behavior of the $Zr–I^{a-i}$ distances appears more structurally related. To a first approximation, these changes can be understood from simple geometry by assuming that the iodine positions remain essentially fixed, perhaps restrained by their matrix effect, while the zirconium octahedra contract upon reduction.

The bonding in these centered clusters may be understood best by initially focusing upon the molecular orbitals derived for an unoccupied cluster and then examining the changes that arise when a carbon atom is included. As noted earlier, the group 5 metal halide clusters $M_6X_{12}^{n+}$ (M = Nb or Ta; X = Cl, Br or I (for Ta); n = 2, 3, or 4) are nominally isostructural with the $Zr_6I^i_{12}$ portion of clusters under study. However, two earlier Hückel-type theoretical studies of the idealized octahedral clusters[15,16] led to two different results. In both, the local coordinate system at each metal atom was chosen so that the z axis was radially directed toward the center of the cluster, while x and y axes pointed toward the four bridging (inner) halides neighboring each metal. With this choice of coordinates, the $d_{x^2-y^2}$ orbital of each metal was set aside for metal–halide bonding, leaving the d_{z^2}, d_{xy}, d_{xz}, and d_{yz} orbitals for metal–metal interactions. Molecular orbitals constructed from these four orbitals will henceforth be denoted as (z^2), (xy), and $(xz\ yz)$, the last pair being degenerate in O_h symmetry. Two major assumptions were made in the earlier calculations to simplify the problem. First, the terminal halides lying exo to each metal vertex were not included because their effect on the bonding of the cluster was assumed to be unimportant. Second, the inner halogen $p\pi$ interactions with the various metal d orbitals were assumed to be equal. To the extent that these assumptions are incorrect, the bonding schemes that arise from these models are also in error.

In the earlier of these studies, Cotton and Haas[15] concluded that the metal–metal bonding orbitals were ordered as $t_{1u}(xz,yz)$ $a_{1g}(z^2)$, $t_{2g}(xz,yz)$, and $a_{2u}(xy)$ in increasing energy. However, errors in the calculation of overlap terms[40] raise questions about the overall correctness of this model. Robbins and thomson[16] repeated Hückel-type calculations for the isolated $M_6X_{12}^{2+}$ cluster using corrected overlap terms and obtained the ordering $a_{1g}(z^2)$, $a_{2u}(xy)$, $t_{1u}(xz,yz)$, and $t_{2g}(xz,yz)$. However, they concluded on the basis of an assignment of magnetic circular dichroism spectra of ethanolic solutions of $M_6X_{12}^{n+}$ (M = Nb or Ta; X = Cl or Br; n = 2, 3, or 4) that these were actually in the order $a_{1g}(z^2)$ $t_{1u}(xz,yz)$, $t_{1u}(z^2)$, and $a_{2u}(xy)$, postulating that crystal field effects, unaccounted for in the Hückel treatment, destabilized the t_{2g}-(xz,yz) and stabilized the $t_{1u}(z^2)$ orbitals.

A. Bonding of Terminal Atoms. In an effort to clarify the bonding of unoccupied M_6X_{12}-type clusters in general, extended Hückel MO calculations were first carried out on a $Zr_6I_{12}^{2+}$ cluster isoelectronic with a hypothetical "Zr_6I_{14}". Since the terminal iodides were thought to be more important in the cluster bonding than previously appreciated, a comparative calculation was then made for the isoelectronic $Zr_6I^i_{12}(I^a)_6^{4-}$ cluster. For simplicity, idealized O_h versions of the observed cluster were used.

The resulting single-electron energies are shown in Figure 4. Although it would be desirable to isolate orbitals involved in Zr–I bonding from those that are simply iodine lone pairs, the high degree of mixing, especially those involving iodine p, makes this extremely difficult. The major contributions to molecular orbitals will be noted when it is possible, but it should be remembered that there are other minor contributions to these. As shown for $Zr_6I_{12}^{2+}$ on the left of the figure, a block of 12 molecular orbitals between −21 and −20 eV is composed of the 12 iodine 5s orbitals with little or no zirconium contribution. The next higher group of 37 molecular orbitals between −13 and −10 eV consists primarily of iodine 5p lone pairs and $Zr–I^i$ bonding combinations, but the one orbital at the top is almost exclusively Zr–Zr bonding, the ra-

(36) Corbett, J. D. *J. Solid State Chem.* **1981**, *37*, 335.
(37) Imoto, H.; Corbett, J. D.; Cisar, A. *Inorg. Chem.* **1981**, *20*, 145.
(38) Voroshilov, Yu. V.; Gorshkova, L. V.; Popova, N. M.; Fedorov, T. F. *Poroshk. Metall.* **1967**, *7*, 81.
(39) Shannon, R. D. *Acta Crystallogr., Sect. A* **1976**, *A32*, 751.
(40) Mingos, D. M. P. *J. Chem. Soc. Dalton* **1974**, 133.

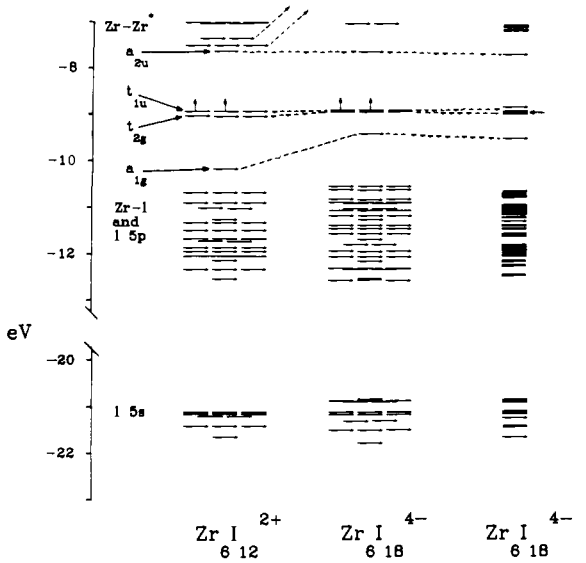

Figure 4. Molecular orbital diagrams from extended Hückel calculations with important Zr–Zr bonding orbitals labeled by symmetry. Left—idealized $Zr_6I_{12}^{2+}$ with O_h symmetry; center—idealized $Zr_6I_{18}^{4-}$ including six terminal iodides; right—distorted $Zr_6I_{18}^{4-}$ with D_{2h} symmetry. The HOMO of the O_h cluster is the t_{1u} set with two electrons. The HOMO of D_{2h} cluster is indicated with an arrow.

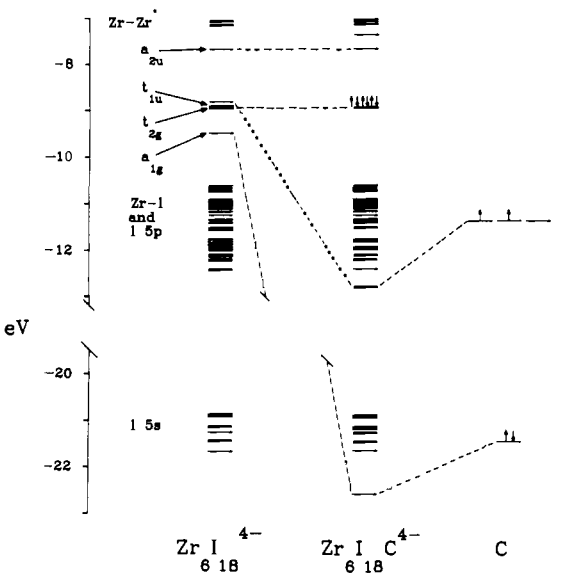

Figure 5. Molecular orbital diagrams from extended Hückel calculations. Left—$Zr_6I_{18}^{4-}$ with D_{2h} symmetry; right—atomic C; center—$Zr_6I_{18}C^{4-}$. Orbital labels are representations in O_h symmetry, and the HOMO of $Zr_6I_{18}C^{4-}$ is the fully occupied t_{2g} set.

dial-based a_{1g} (z^2). The next seven orbitals are also primarily involved in Zr–Zr bonding. These then are the eight Zr–Zr bonding orbitals that would be filled in a hypothetical 16-electron O_h cluster like $Ta_6I_{12}^{2+}$ in the order $a_{1g}(z^2)$, $t_{2g}(xz,yz)$, $t_{1u}(xz,yz)$, and $a_{2u}(xy)$. The axially directed $e_g(z^2)$ and $t_{1u}(z^2)$ are not very effective at cluster binding and lie at a slightly higher energy (−7.5 eV) than the eight just cited. While the reordering of the $t_{2g}(xz,yz)$ and $t_{1u}(z^2)$ postulated by Robbins and Thomson may seem at least plausible in an isolated $M_6X_{12}^{n+}$ cluster, the effect of the six terminal halides (or solvent molecules such as ethanol) makes this highly improbable.

As seen in the center of Figure 4, the inclusion of the six terminal iodides strongly affects the three Zr–Zr molecular orbitals originating from the metal d_{z^2} atomic orbitals, $a_{1g}(z^2)$, $e_g(z^2)$, and $t_{1u}(z^2)$.[41] This might be expected since the σ-bonding p_z orbitals on these iodines transform the same as and have an energy comparable to those of the d_{z^2} metal orbitals. This interaction generates three new Zr–I^a bonding orbitals that lie below the primarily Zr–Zr bonding orbitals plus three combinations at higher energy that are Zr–I^a antibonding but Zr–Zr bonding. Of these three, the $a_{1g}(z^2)$ MO moves to higher energy but remains the lowest metal–metal bonding orbital at about −9.6 eV. Because of similarly strong σ interactions, the other two metal–metal bonding orbitals, $e_g(z^2)$ and $t_{1u}(z^2)$, move off-scale to energies several electronvolts above the values obtained without the terminal iodines. Thus, the metal–metal bonding scheme resulting from the inclusion of the six terminal iodines is much more peripheral in nature than that proposed by Robbins and Thomson, as the occupied $t_{1u}(xz,yz)$ molecular orbital is more or less centered on the faces of the octahedron in contrast to the axial character of the $t_{1u}(z^2)$ orbitals. In contrast, only slight increases in energies of the Zr–Zr $t_{2g}(xz,yz)$ and, to a lesser extent, of the $t_{1u}(xz,yz)$ orbitals are found upon inclusion of the six terminal iodines, these changes originating with π-antibonding interactions with the terminal iodine p_x,p_y set.

The omission of terminal chlorine atoms in the EHMO calculations made on $Nb_6Cl_{12}^{2+}$ by Voronovich and Korol'kov[42] is presumably responsible for their erroneous conclusion that the HOMO is e_g^2. The a_{2u}^2 HOMO level indicated by the present calculation is consistent with the known nondegeneracy of that level according to the magnetic properties of the 2+, 3+, and 4+ niobium chloride clusters isolated as the hexachloro anions.[43] The importance of terminal atom bonding is also seen clearly in calculations that have been made on M_6X_8-type clusters where the nonmetal is face-capping. The addition of terminal ligands to such a cluster again greatly decreases the binding energies of the comparable t_{1u} and e_g molecular orbitals (Figure 4). This was first noted for the unsymmetrical cluster in $(Mo_6Br^i_8)Br^a_4(H_2O^a)_2$.[44] The same effect has also been described[45] for Mo_6S_8 and larger clusters on the addition of six terminal sulfide ligands, analogous to the behavior in the solid state in Chevrel phases where the terminal sulfur atoms are simultaneously face-capping in other clusters.

The σ bonding of the six terminal halide ligands to M_6X_{12}- or M_6X_8-type clusters that strongly affects the molecular orbital scheme within the cluster also provides plausible explanations for cluster distortions when the terminal atoms are not all of the same character, as we shall see shortly. That these terminal ligand interactions must also be energetically important follows from general observations[46] that virtually all octahedral metal cluster halides as well as extended arrays derived by cluster condensation always have these terminal positions occupied, even if otherwise well-bonded inner halides must be used for this purpose.

Finally, the effects of distortion of the actual cluster in $Zr_6I_{14}C$ from O_h to D_{2h} symmetry plus small changes in distances are seen in the molecular orbital diagram for $Zr_6I_{18}^{4-}$ on the right side of Figure 4. Although the degeneracy of many orbitals is removed, the changes are no more than 0.1 eV, and so the MO's in the lower symmetry will continue to be referred to in their O_h-equivalent descriptions to simplify the discussion.

B. Bonding of Carbon. A comparable extended Hückel calculation on a $Zr_6I_{18}C^{4-}$ cluster using the coordinates obtained for $Zr_6I_{14}C$ gave results shown in the center of Figure 5 with the earlier diagram for the distorted but empty $(Zr_6I_{12})I_6^{4-}$ cluster on the left. The strong interactions between the carbon $2s(a_{1g})$ and $2p(t_{1u})$ orbitals with Zr–Zr (and Zr–I^a) bonding orbitals of like symmetry give four rather strongly bonding orbitals and four antibonding orbitals at higher energy (off-scale). Not surprisingly, the two occupied $a_{1g}(z^2)$ orbitals undergo considerable rehybridization on inclusion of carbon 2s. The lowest-lying (−22.8 V) a_{1g} level is comprised mostly of carbon 2s with some zirconium

(41) A similar observation has been made by: Hughbanks, T.; Burdett, J., private communication, 1984.
(42) Voronovich, N. S.; Korol'kov, D. V. *Russ. J. Struct. Chem.* **1971**, *12*, 676.
(43) Koknat, F. W.; McCarley, R. E. *Inorg. Chem.* **1974**, *13*, 295.
(44) Guggenberger, L. J.; Sleight, A. W. *Inorg. Chem.* **1969**, *8*, 2041.
(45) Hughbanks, T.; Hoffmann, R. *J. Am. Chem. Soc.* **1983**, *105*, 1150.
(46) Corbett, J. D. unpublished observations, 1984.

d_{z^2} contribution but little terminal iodine p_z component. The a_{1g} orbital that is Zr–I^a bonding no longer contains significant zirconium $a_{1g}(z^2)$ and is essentially nonbonding within the cluster (−11.5 eV). The third combination is Zr–C antibonding and occurs at very high energy. The Zr–C bonding derived from the zirconium $t_{1u}(xz,yz)$ set and carbon p orbitals is largely π in character (though not entirely), and the MO again contains little or no contribution from the terminal iodine orbitals. The result is that changes in the Zr–I^a distances, and thence bonding have little or no *direct* effect on Zr–C bonding.

The effect of the inclusion of the carbon atom is that the carbon "donates" its valence electrons to the bonding cluster MO's, affecting the energies but not the number of bonding orbitals since four new antibonding levels are also formed. While this "donation" is useful in electron counting,[47] a charge transfer should *not* be inferred. Rather the bonding is quite covalent, with somewhat more carbon 2s and 2p than Zr contribution in the four new orbitals formed so that the charge on the carbon is negative, about −1.8 according to the calculations. Though this estimate is likely an exaggeration, it most certainly is correct in sign. The stabilizing effect of the interstitial carbon is the strong interaction of the s and p orbitals with a subset of the Zr–Zr cluster orbitals. A significant metal–carbon covalency and a carbidic character of the carbon are evident in the XPS data for $Sc_7Cl_{10}C_2$, Sc_2Cl_2C, and Zr_2X_2C, X = Cl or Br.[20,48]

The 14-cluster-based electrons in $Zr_6I_{14}C$ fill the a_{1g} and t_{2u} orbitals, which are primarily Zr–C bonding but which retain some Zr–Zr bonding as well, and the t_{2g} orbitals, as shown, which are mainly Zr–Zr bonding. Occupation of the eighth (a_{2u}) orbital on further reduction appears to produce first a decrease in the average Zr–Zr distance of ~0.03 Å for $CsZr_6I_{14}C$ and then a larger drop of 0.09 Å for $Zr_6I_{12}C$, there being slight increases in the Zr–I^a or Zr–I^{i-a} distances at the same time. The number of electrons involved in the cluster bonding in these carbides is exactly the same as in the well-known and interstitial-free group 5 examples, and, not surprisingly, trends in bond distances on reduction of the isolated $Nb_6Cl_{18}^{n-6}$ cluster anions[10] are similar, but clearly without the discontinuity in metal–metal distances realized on addition of the sixteenth electron in $Zr_6I_{12}C$. Since the a_{2u} molecular orbitals being filled at this point are presumably similar, the dramatic effect on Zr–Zr distances in the zirconium series must be related to the change in structure type.

C. Cluster Distortions. The major structural difference between the $Zr_6I_{14}C$ and $Zr_6I_{12}C$ structures is the replacement of four relatively short Zr–I^{a-a} distances in the former with longer Zr–I^{a-i} distances in the latter. At the same time, the tetragonal compression of the cluster found in $Zr_6I_{14}C$ disappears, and the result is close to O_h symmetry. This too is not solely the result of the number of electrons involved, since the 16-electron clusters in Ta_6I_{14}[11] and Nb_6Cl_{14}[12] also show the same tetragonal compression found here with fewer electrons, while the clusters in $Nb_6Cl_{18}^{2-}$,[10] Ta_6Cl_{15},[13] Ta_6I_{15},[49] and $Nb_6Cl_{18}^{4-}$[50] which contain 14, 15, 15, and 16 cluster electrons, respectively, and either symmetric or no bridging terminal halides are all close to octahedral symmetry. Evidently changes in the length of the M–X^a or M–X^{a-i} interactions have an inverse effect on M–M bonding within the cluster.

To determine the effect of the different terminal halide functions and distances on metal–metal bonding, extended Hückel calculations were made for both unoccupied and carbon-centered clusters with geometries similar to that of the distorted $Zr_6I_{18}^{4-}$ cluster discussed above. However, the four iodines at distances appropriate to I^{a-a} were moved to longer distances to represent the Zr–I^{a-i} bridging in Zr_6I_{12}-type structures, or two more distant I^{a-i}-type atoms were moved to shorter distances as found for all six terminal X^a halides in M_6X_{15} (=$M_6X_{12}X_{6/3}$) and $M_6X_{18}^{4-}$ compounds. Analysis of the atomic orbital contributions to the cluster MO's shows conclusively that shorter Zr–I^a distances in the latter types lead to a greater metal contribution to the Zr–I^a bonding and to a corresponding decrease in the Zr–Zr bonding, correlating with the expansion observed about the cluster waist (Zr1, Figure 2*b*) in all M_6X_{14} phases. Conversely, longer Zr–I^a distances represent a smaller zirconium contribution to terminal atom bonding and correspondingly stronger Zr–Zr bonding, as in $Zr_6I_{12}C$. The change in Zr–Zr bonding in an empty cluster occurs almost exclusively in the Zr–Zr $a_{1g}(z^2)$ orbital, but the inclusion of carbon in the clusters changes this rather dramatically. The Zr–C $a_{1g}(z^2)$ orbital (because there is negligible I^a contribution) is unaffected by differences in Zr–I^a bonding. As a result, changes in Zr–Zr bonding are more diffuse but still evidenced by differences in reduced overlap popualtions for Zr–Zr interactions. Thus, in $Zr_6I_{12}C$ where the Zr–I^{a-i} bonds are all the same length and significantly longer, the cluster is not only more symmetric but also has stronger Zr–Zr and Zr–C bonding. While not explicitly predicted by the calculations, a synergistic increase in Zr–C bonding must result from the increase in Zr–Zr bonding and the decrease in Zr–Zr distances. One may expect, therefore, that clusters with only one type of terminal ligand will have nearly octahedral metal cores, while those with more asymmetric terminal ligands will show distortions because of interrelated metal–terminal ligand and metal–metal bonding effects. Such a distortion is also seen in the cluster $(Mo_6Br_8)Br_4\cdot 2H_2O$.[42]

A requirement of 14–16 electrons for the stability of M_6X_{12}-type clusters at present seems fairly general. Interstitial atoms are one way to achieve this. Niobium and tantalum attain these counts in binary halides, while the zirconium analogues, which would as binary phases contain only 10 to 12 electrons, achieve this sum with the aid of a centered carbon (or other) atom. Four metal–metal bonding orbitals, not necessarily already occupied, are thus altered by including strong metal–carbon bonding (although some metal–metal bonding components are also retained. The size as well as the electron count of the interstitial would thus seem to be important so that the three or four metal–metal bonding orbitals remaining are not greatly weakened although the strength of the metal-interstitial bonding is probably dominant. The 14-electron counts have also been achieved with interstitial atoms in other cluster arrangements, for example, $(Zr_6Cl_{12}N)Cl_{6/2}$, $Sc(Sc_6Cl_{12}N)$,[24] $Zr_6Cl_{13}B$, and $KZr_6Cl_{15}C$.[21] Other phases and other interstitial atoms are currently under investigation in these systems.

Acknowledgment. We express our appreciation to Dr. R. A. Jacobson and his group for continuing X-ray crystallographic servies, to Dr. K. A. Gschneidner and R. Stierman for their assistance in obtaining the magnetic susceptibility data, and to Dr. S. Wijeyesekera for help in obtaining and interpreting the extended Hückel results.

Supplementary Material Available: Tabulations of the anisotropic temperature factors, the observed and calculated structure factors for the four structures studied, and atomic coordinates and orbital parameters used in the extended Hückel calculations (16 pages). Ordering inforamtion is given on any current masthead page.

(47) Lauher, J. W. *J. Am. Chem. Soc.* **1978**, *100*, 5305.
(48) Hwu, S.-J.; Ziebarth, R. P.; Winbush, S. v.; Ford, J. E.; Corbett, J. D. *Inorg. Chem.*, submitted.
(49) Bauer, D.; Schäfer, H. *J. Less-Common Met.* **1968**, *14*, 476.
(50) Simon, A.; von Schnering, H.-G.; Schäfer, H. *Z. Anorg. Allg. Chem.* **1968**, *361*, 235.